Arterial endothelial deletion of *Alk1* causes epistaxis and cerebral microhemorrhage with aberrant arteries and defective smooth muscle coverage.

Xuetao Zhang, PhD[1,2†]; Kyle A Jacobs, BS[1,2,3†]; Kunal P Raygor, MD[1,2,‡]; Shang Li, PhD[1,2]; Jiajun Li[1,2]; Rong A Wang, PhD[1,2,✉]

[1] Laboratory for Accelerated Vascular Research, Department of Surgery, University of California, San Francisco; San Francisco, CA 94143.
[2] Cardiovascular Research Institute, University of California, San Francisco; San Francisco, CA 94143.
[3] Biomedical Sciences Graduate Program, University of California, San Francisco; San Francisco, CA 94143.
[†] These authors contributed equally to this work.
[‡] Present address: Department of Neurological Surgery, Vanderbilt University Medical Center; Nashville, TN 37232

Hereditary Hemorrhagic Telangiectasia (HHT) is an autosomal dominant vascular disorder with presentations including severe nose bleeding and microhemorrhage in brains. Despite being the second most common inherited bleeding disorder, the pathophysiological mechanism underlying HHT-associated hemorrhage is poorly understood. Mutations in activin receptor-like kinase 1 (*ALK1*) gene cause HHT type 2. HHT pathogenesis is thought to follow a Knudsonian two-hit model, requiring a second somatic mutation for lesion formation. We hypothesize that somatic mutation of *Alk1* in arterial endothelial cells (AECs) leads to arterial defects and hemorrhage. Here, we investigate the effects of *Alk1* mutation in AECs in mice, using *Bmx(PAC)-Cre^{ERT2}*-mediated postnatal somatic mutation. We mutated *Alk1* in primarily AECs and found that somatic arterial endothelial mutation of *Alk1* is sufficient to induce spontaneous epistaxis and multifocal cerebral microhemorrhage. Interestingly, this bleeding occurred in the presence of tortuous and enlarged blood vessels, loss of arterial molecular marker *Efnb2*, disorganization of vascular smooth muscle, and impaired vasoregulation. Our data suggest that arterial endothelial mutation of *Alk1* causing reduced arterial identity and disruption of vascular smooth muscle cell coverage is a plausible molecular mechanism for HHT-associated severe epistaxis. This work provides the first evidence that somatic ALK1 loss in AECs can cause hemorrhagic vascular lesions, offering a novel preclinical model critically needed for studying HHT-associated epistaxis, and delineating an arterial mechanism to HHT pathophysiology.

✉Corresponding author: Rong.Wang@ucsf.edu

Introduction

Hereditary hemorrhagic telangiectasia (HHT) is an autosomal dominant vascular disorder characterized by bleeding and malformations of blood vessels[1,2]. One of the most common clinical HHT presentations, and one of the major diagnostic criteria[1], is severe recurring epistaxis, or nose bleeding, which was reported to occur in up to 96% of HHT patients[3]. The severity of bleeding in HHT patients frequently leads to secondary complications, such as anemia, in upwards of 50% of patients[4]. HHT patients additionally present with multifocal arteriovenous malformations (AVMs), blood vessels that shunt arterial blood directly into veins without passing through the capillaries[5,6], of the brain[7] and other tissues[2]. These peripheral AVMs can result in vascular shunting and subsequent development of high-output cardiac failure which increases the risk of HHT-associated mortality[8]. Despite these consequential impacts on HHT patient quality of life, there are no FDA- or EMA-approved therapeutics or prophylactics for HHT-associated bleeding and patients often require surgical intervention to address bleeding lesions.

The pathological basis of epistaxis is not well understood. Epistaxis in HHT patients typically originates from Little's area, also known as Kiesselbach's plexus, a vascular plexus on the anterior nasal septum formed by the anastomosis of the anterior and posterior ethmoidal arteries, the sphenopalatine artery, the greater palatine artery, and the superior labial artery[9,10]. The nasal vasculature of children with a parent affected by HHT exhibits both focal telangiectasias and varicose vessels[11]. The data indicate that in some patients, no telangiectasias were detected in the nose, however the patient nonetheless developed recurrent epistaxis[11]. These clinical findings of epistaxis with undetectable telangiectasia raise question of other vascular causes of epistaxis. It is also unclear whether severity of epistasis correlate to the size of nasal telangiectasia. Furthermore, defects in arterial flow is likely to explain severe bleeding. Therefore, it is a reasonable to question whether lesions in feeding artery may be a cause for epistaxis.

HHT type-2 (HHT2) is a subtype of HHT characterized by germline inheritance of a mutated copy of *ALK1/HHT2*[12–14]. ALK1, or activin receptor-like kinase 1, is a receptor tyrosine kinase in the TGFβ/BMP pathway[15]. Mouse models have been instrumental in developing an understanding of the genetic underpinnings of HHT-associated vascular malformations [16,17]. While germline loss of *Alk1* is embryonic lethal by E10.5 in mice[13], *Alk1*$^{+/-}$ mice are fertile and viable and may develop vascular malformations with low frequency and latency[18]. Studies examining the effects of post-natal, somatic *Alk1* mutation utilizing tissue-specific mouse genetic strategies have been facilitated the generation of an *Alk1*-floxed allele[19]. Interestingly, homozygous mutation of *Alk1* mediated by *L1cre*, a transgenic *Alk1* promoter-driven Cre allele, resulted in AVMs and embryonic lethality by E18.5[19]. *Alk1* mutation using *Rosa26Cre*^{ER} determined that global *Alk1* loss postnatally causes de novo AVMs in response to tissue injury and subsequent moribundity[20]. Additional work utilizing the *Cdh5(PAC)-Cre*^{ERT2} to induce postnatal mutation of *Alk1* specifically in endothelial cells is sufficient to induce the formation of retinal AVMs[21,22]. Despite these progresses, a mouse model of HHT-associated epistaxis has not been reported. Thus, there is a critical need for such model to interrogate mechanisms leading to vascular hemorrhage and inform the development of novel HHT therapeutics and prophylactics.

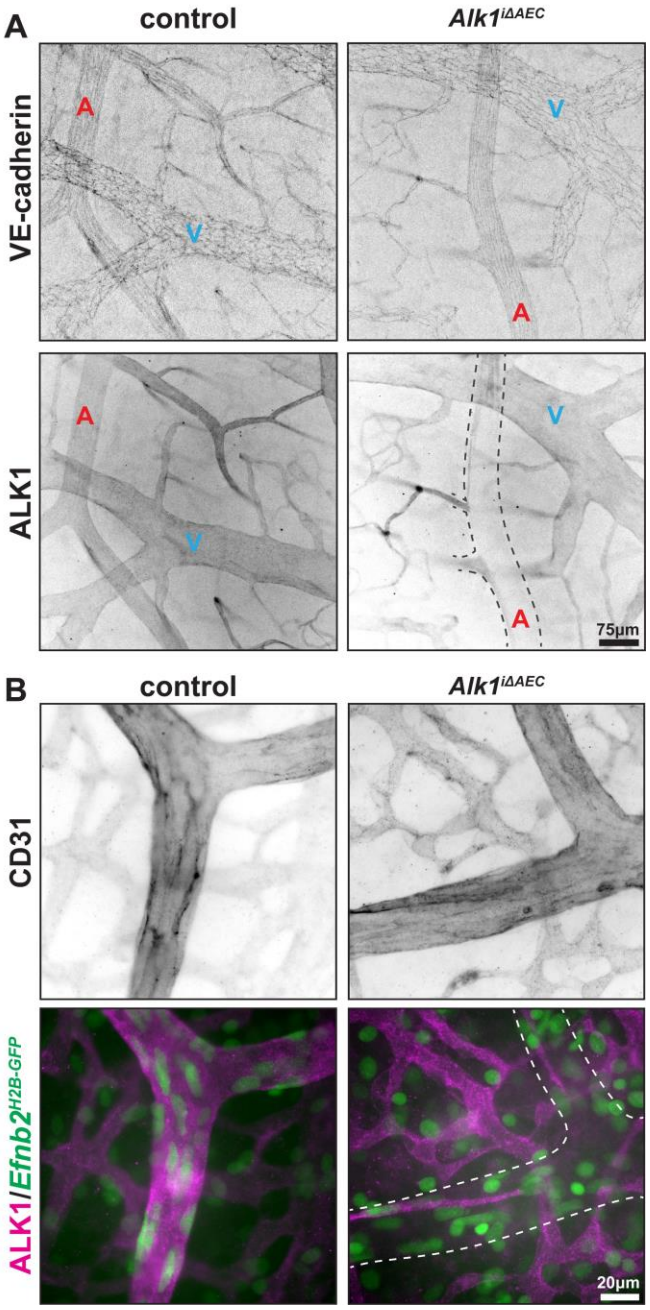

Fig. 1 | *Bmx(PAC)-Cre*^{ERT2} mediated loss of ALK1 was restricted to arterial endothelium. (A) Wholemount immunostaining of cerebral cortex slices for VE-cadherin and ALK1 from P31 control and *Alk1*^{iΔAEC} mice (25μg tamoxifen on P2). **(B)** Wholemount immunostaining for CD31 and ALK1 in cerebral cortex slices of P10 control and *Alk1*^{iΔAEC} mice expressing *Efnb2*$^{H2B-GFP}$ (50μg tamoxifen on P2). A and V label arteries and veins, respectively. Dashed outlines in ALK1 images indicate artery position.

HHT2 exhibits an autosomal dominant pattern of inheritance, meaning that all cells in the body lack a functional copy of *ALK1*. However, vascular malformations in HHT patients appear focally and stochastically, not systemically throughout the vasculature. This dichotomy has led the hypothesis that HHT-associated vascular malformations may follow a Knudsonian, two-hit model of inheritance, whereby a second somatic mutation is required for the development of a vascular malformation[23,24]. Recent work has utilized next generation sequencing to investigate loss of heterozygosity events in HHT AVMs and identified somatic mutations which support this bi-allelic two-hit mutation model[25,26]. Since this second somatic mutation may occur in any cell of the vasculature, these findings raise pressing questions as to how the site of the somatic mutation may impact phenotypic presentation. Previous work has elegantly demonstrated that loss of HHT genes in venous and capillary endothelial cells leads to the development of AVMs in mice and zebrafish[27–31]. Here we investigate the arterial contribution to HHT pathogenesis and ask whether somatic mutation of *Alk1* in the arterial endothelium is sufficient to induce formation of HHT-associated vascular malformations.

To examine the role of ALK1 in arterial endothelial cells (AECs) in driving HHT pathogenesis, we utilized mice expressing the *Bmx(PAC)-Cre*^{ERT2} allele to induce mutation of *Alk1* in primarily AECs of postnatal mice[27,32]. Excitingly, somatic mutation of *Alk1* in AECs caused spontaneous epistaxis and cerebrovascular hemorrhage, malformed arteries with defective arterial specification, smooth muscle coverage, and vasoregulation. This new-found appreciation of the arterial contribution to HHT pathogenesis in mice may inspire future studies into arterial contribution to bleeding in HHT patients.

Results

Somatic loss of ALK1 in cells of the *Bmx(PAC)-Cre*^{ERT2} lineage induced epistaxis and cerebral microhemorrhage.

To determine the effects of loss of *Alk1* in arterial endothelial cells in mice, we somatically mutated both *Alk1* alleles in the cells of the *Bmx(PAC)-Cre*^{ERT2} lineage, which

consists primarily of arterial endothelial cells[27,32]. We activated *Bmx(PAC)-Cre*^{ERT2} activity in mice with both *Alk1* alleles flanked by loxP sites (*Bmx(PAC)-Cre*^{ERT2}; *Alk1*$^{fx/fx}$, hereafter *Alk1*$^{i\Delta AEC}$). As controls, we used mice carrying *Alk1*$^{fx/fx}$ without the *Bmx(PAC)-Cre*^{ERT2} allele (hereafter control).

To evaluate the *Bmx(PAC)-Cre*^{ERT2} recombinase-mediated loss of ALK1, we conducted wholemount immunostaining for ALK1 in the cerebral cortex of postnatal day (P) 31 *Alk1*$^{i\Delta AEC}$ and control mice injected with 25µg tamoxifen on P2 (**Fig. 1A**). We found that *Alk1*$^{i\Delta AEC}$ mice exhibited loss of ALK1 in the arteries but retained ALK1 in the veins and capillaries. We also performed ALK1 immunostaining in the cerebral cortex of P21 *Alk1*$^{i\Delta AEC}$ and control mice injected with 100µg tamoxifen on P2 and P3 and show similar loss of ALK1 in the arteries but not in the veins and capillaries (**Supplemental Fig. 1**). To further confirm the arterial specificity of ALK1 loss, we used *Alk1*$^{i\Delta AEC}$ and control mice also carrying the *Efnb2*$^{H2B\text{-}GFP}$ arterial endothelial reporter[33]. This allele expresses Histone H2B-GFP under the endogenous *Efnb2* promoter, thereby labeling the nuclei of arterial, but not capillary or venous, endothelial cells[33]. Indeed, we find that ALK1 loss is restricted to vessels with nuclear GFP signal (**Fig. 1B**). Taken together, these data demonstrate the arterial endothelial specificity of ALK1 protein depletion in *Alk1*$^{i\Delta AEC}$ mice.

Alk1$^{i\Delta AEC}$ mice exhibited spontaneous episodes of epistaxis from about 4 weeks of age (**Fig. 2A**). Epistaxis

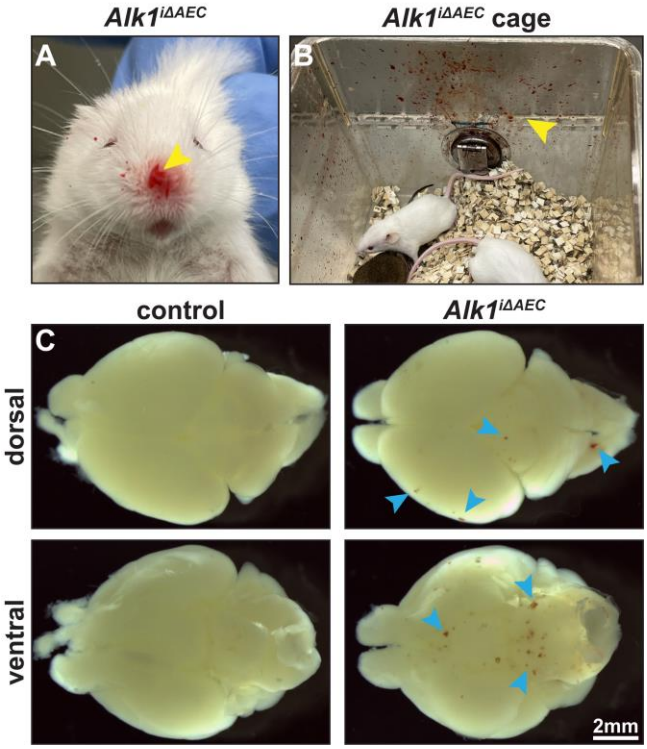

Fig. 2 | *Alk1*$^{i\Delta AEC}$ mice exhibited epistaxis and brain hemorrhage. **(A)** Photograph of P33 *Alk1*$^{i\Delta AEC}$ mouse with blood on nose (arrowhead). **(B)** Photograph of blood present (arrowhead) in cage housing P81 *Alk1*$^{i\Delta AEC}$ mice. **(C)** Gross pathological images demonstrating multi-focal hemorrhages (arrowheads) present in *Alk1*$^{i\Delta AEC}$ mice brains but absent in control at P7. All mice administered 25µg tamoxifen on P2.

episodes were first identified during daily health checks wherein blood was found dripped on bedding or sprayed on cage walls (**Fig. 2B**). Subsequently, we discovered epistaxis or blood on bedding/cage walls in 47.6% of cages containing *Alk1*$^{i\Delta AEC}$ mice (N=21 cages, both male and female mice). We also randomly identified mice with blood on the tips of their noses (**Fig. 2A**). Fortuitously, we found that upon holding the mice for examination, epistaxis would frequently occur (**Supplemental Movie 1**), enabling us to identify the nose as the source of bleeding. These epistaxis events were transient in nature with the bleeding quickly stopping and mice rapidly cleaning the blood off the nose. With this transient bleeding, *Alk1*$^{i\Delta AEC}$ mice lived and continued exhibiting epistaxis as long as we kept them (longest is P195). As epistaxis occurs in up to 96% of HHT patients, *Alk1*$^{i\Delta AEC}$ mice resembled patients with nosebleed.

To determine the brain phenotypes in *Alk1*$^{i\Delta AEC}$ mice, we conducted necropsies to assay for hemorrhage in the brain. Interestingly, the *Alk1*$^{i\Delta AEC}$ mice displayed the presence of multifocal microhemorrhages located throughout the brain with an incidence of 72.4% of *Alk1*$^{i\Delta AEC}$ mice (N=58 mice; **Fig. 2C**). We noted no significant difference in incidence cerebral vascular hemorrhage in male and female *Alk1*$^{i\Delta AEC}$ mice. Thus, arterial endothelial loss of ALK1 is sufficient for the development of multifocal microhemorrhages. As patients with HHT2 also develop multifocal microhemorrhages in the brain[34], *Alk1*$^{i\Delta AEC}$ mice closely resembled this phenotypic presentation.

A viable mouse model of HHT2 with epistaxis and cerebral microhemorrhage exhibited dermal telangiectasias and compensatory cardiac failure.

In optimizing this preclinical model, our objective was to identify permissive conditions in which mice developed epistaxis and other vascular abnormalities without developing secondary systemic comorbidities that lead to declined health and moribundity shortly after *Alk1* mutation. To this end, we tested four different tamoxifen doses for Cre recombinase induction (25, 50, 75, and 100µg). We found that at high dose (100µg on P2 and P3), *Alk1*$^{i\Delta AEC}$ mice developed malformations described here, however rapidly became moribund (median 23 days; **Fig. 3**). Low dosing of tamoxifen (25µg) led to slower onset of and milder phenotype, however, was competent to induce vascular malformations. Low tamoxifen doses very rarely caused systemic illness, and thus were used for most of our investigations. We likewise administered 50µg and 75µg tamoxifen on P2; these doses resulted in the same vascular phenotypes as 25µg but with variable severity. Together, this dosing strategy provides the framework for an HHT model with tamoxifen-titratable phenotypic severity.

HHT patients can develop high-output heart failure due to peripheral vascular shunting[35]. To evaluate cardiomegaly, an indicator of high-output cardiac failure, we documented heart to body weight ratio, which reflects cardiomegaly. We found that *Alk1*$^{i\Delta AEC}$ mice over two weeks of age developed an enlarged heart and a greater heart weight to body weight ratio relative to controls when tamoxifen is administered at P2 (**Supplemental Fig. 2**). Because *Alk1*$^{i\Delta AEC}$ mice develop

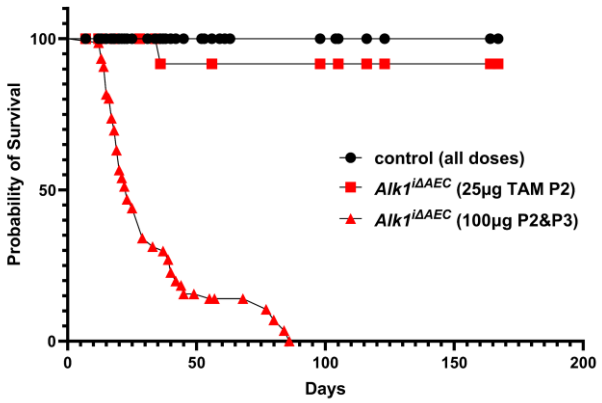

Fig. 3 | *Alk1*$^{i\Delta AEC}$ mice exhibited tamoxifen dose-dependent moribundity. Kaplan-Meier analysis showed that time to moribundity in *Alk1*$^{i\Delta AEC}$ mice administered 100µg tamoxifen on P2 and P3 (red triangles) was significantly faster (median 23 days) than control (black circles) and *Alk1*$^{i\Delta AEC}$ mice administered 25µg tamoxifen on P2 (N = 45-80 mice per condition).

brain hemorrhages as early as P7 when tamoxifen is administered at P2 (**Fig. 2C**), we examined mice between P7 and P15, to determine if a change in heart size succeeds vascular phenotypes. We found no significant difference in heart weight to body weight ratio in mice younger than 15 days old (**Supplemental Fig. 2**), indicating that changes in vascular phenotype preceded compensatory cardiomegaly development. The development of compensatory high-output cardiac failure in *Alk1*$^{i\Delta AEC}$ mice demonstrates further that arterial endothelial loss of ALK1 is an excellent model to recapitulate many HHT phenotypes observed in patients.

In *Alk1*$^{i\Delta AEC}$ mice we observed the formation of dermal vascular malformations, like seen in HHT patients[36]. These vascular malformations were most evident on the dorsal aspect of the head of *Alk1*$^{i\Delta AEC}$ mice (**Supplemental Fig. 3**) and presented heterogeneously, with some being focal, and others being diffuse tangles of tortuous vessels. Thus, administering *Alk1*$^{i\Delta AEC}$ mice high doses of tamoxifen enables the modeling and analysis of dermal vascular malformations, further validating the model's phenotypic similarity to human.

To address whether deletion at later timepoint is sufficient to induce phenotypic presentation, we administered 100µg tamoxifen per g body weight at P13 and P14 and sacrificed mice at 14 weeks of age. We found these mice exhibited epistaxis (**Supplemental Fig. 4A**) and cardiomegaly with average heart weight to body weight ratio of *Alk1*$^{i\Delta AEC}$ and control mice being 0.010 and 0.0045, respectively (N=2 *Alk1*$^{i\Delta AEC}$ mice; **Supplemental Fig. 4B**).

In summary, we show that Cre recombinase induction by injection of 25µg tamoxifen on P2 leads to a progressive phenotypic development over a prolonged period with ongoing transient epistaxis, while higher dose leads to a quicker phenotypic onset and more uniform phenotypes at a given time.

Alk1$^{i\Delta AEC}$ mice exhibited blood vessel enlargement and tortuosity.

Given the spontaneous bleeding in *Alk1*$^{i\Delta AEC}$ mice, we sought to determine gross changes in the nasal vasculature contributing to the development of hemorrhage. Using a combination of MICROFIL vascular casting and gross observation, we determined that bleeding in *Alk1*$^{i\Delta AEC}$ mice occurs in the presence of tortuous and enlarged major vessels without the development of obvious nidi with tangled enlargement of arterial-venous connection.

It is well established that most human epistaxis is caused by hemorrhage of the vasculature of Little's area/Kiesselbach's plexus[9,10]. To visualize the feeding arteries and draining veins of the murine structure analogous to Little's area we casted *Alk1*$^{i\Delta AEC}$ and control mice using MICROFIL and optically cleared the head to visualize blood vessels on the cranial exterior. We discovered a significant enlargement of the facial artery/vein and their tributaries in the mutant mice. We furthermore identified a bed of tortuous blood vessels in the distal nasal plate, which was not detectable in control mice (**Fig. 4A**). Thus, by vascular casting we demonstrate significant vascular enlargement and tortuosity in the head of *Alk1*$^{i\Delta AEC}$ mice.

To further investigate the vascular defects within the nasal cavity where bleeding was occurring, we conducted wholemount immunofluorescent staining of the nasal mucosa of *Alk1*$^{i\Delta AEC}$ and control mice which revealed large vessels within the nasal mucosa to be enlarged and tortuous. Interestingly, the vessels exhibiting enlargement were arteries which had undergone Cre-mediated recombination and loss of ALK1, as demonstrated by expression of the *Rosa26*^{Ai75} Cre recombinase reporter (**Fig. 4B**). Taken together, these results indicate that bleeding in *Alk1*$^{i\Delta AEC}$ mice occurs in the presence of enlarged and tortuous major vessels.

We likewise sought to interrogate the vascular patterning of the cerebral cortex where multifocal hemorrhages formed in *Alk1*$^{i\Delta AEC}$ mice. To visualize the vasculature of the brains of *Alk1*$^{i\Delta AEC}$ and control mice, we conducted MICROFIL casting which revealed that the vessels of *Alk1*$^{i\Delta AEC}$ mice are significantly more tortuous than those of the control (**Fig. 5A**). To investigate this phenotype in higher resolution using a complimentary modality, we immunostained the cerebral cortex of *Alk1*$^{i\Delta AEC}$ and control mice for CD31 and confirmed that the large vessels exhibit significant tortuosity (**Fig. 5B**). Thus, we find that arterial endothelial mutation of *Alk1* is sufficient to drive the development of large vessel tortuosity in the brain.

Alk1$^{i\Delta AEC}$ mice exhibited vascular smooth muscle cell defects.

Large tortuous blood vessels have been described in multiple diseases including Loeys-Dietz syndrome, Marfan's syndrome, and Arterial Tortuosity syndrome, all of which are disorders affecting the integrity of the tunica media and vascular smooth muscles[37,38]. With this insight, we sought to examine the effects of arterial endothelial *Alk1* loss on vascular smooth muscle cell (vSMC) function. We conducted wholemount immunostaining for α-smooth muscle actin (αSMA) in the nasal mucosa of *Alk1*$^{i\Delta AEC}$ mice. We found that, the *Alk1*$^{i\Delta AEC}$ mouse nasal vessels exhibited holes in arterial vSMC coverage (**Fig. 6A**). Likewise, wholemount immunostaining for αSMA in the cerebral cortex revealed a

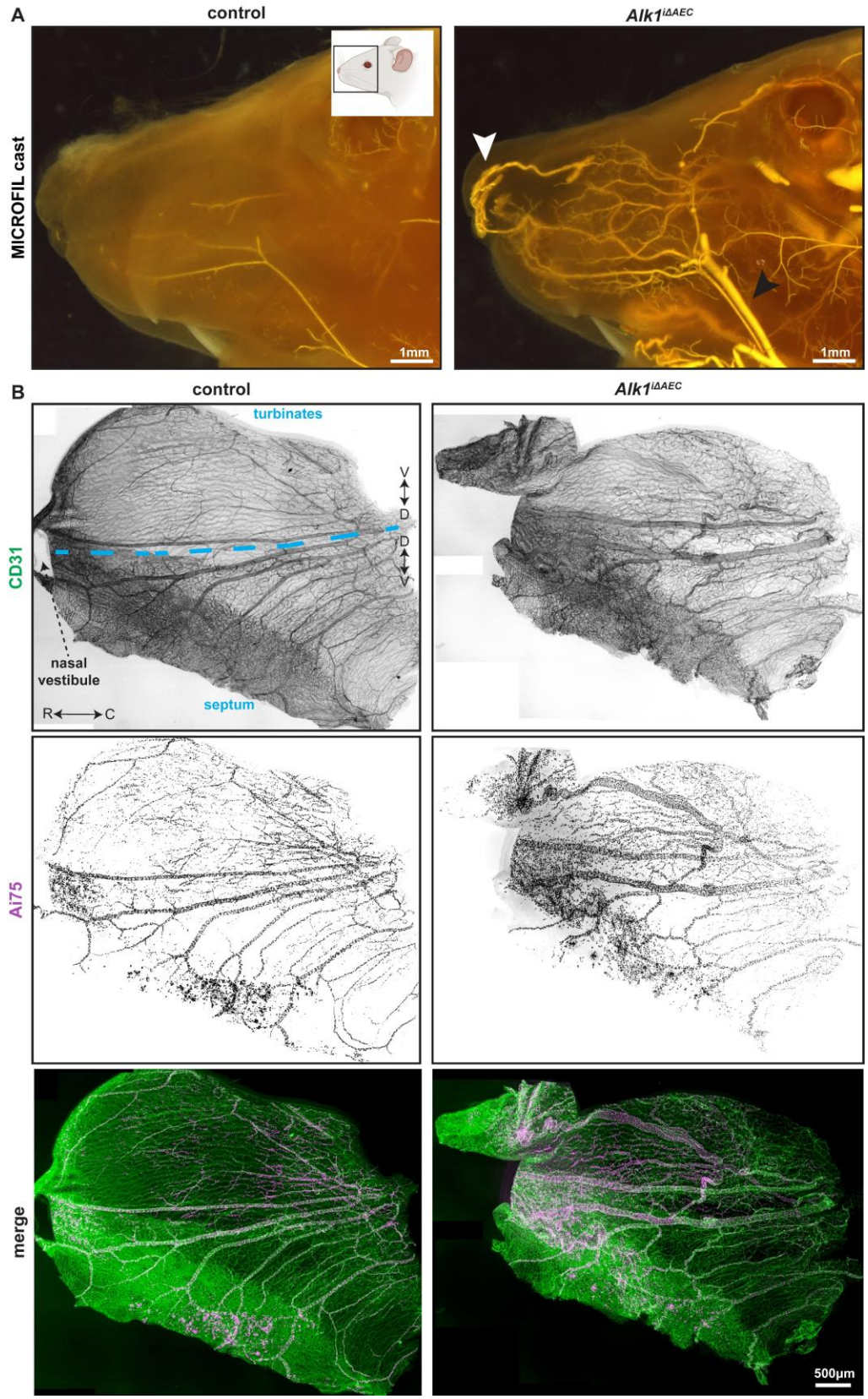

Fig. 4 | *Alk1*^{iΔAEC} mice exhibited enlarged and tortuous nasal vasculature. (A) MICROFIL casting of nasal cavity and cranial exterior of control (P16) and *Alk1*^{iΔAEC} (P19) mice revealed enlarged and tortuous vessels in *Alk1*^{iΔAEC} mouse (100μg tamoxifen on P2 & P3). Black and white arrowheads indicate the facial artery/vein pair and a tangle of blood vessels in the distal nasal vestibule, respectively. Mouse schematic created in BioRender.com. **(B)** Wholemount immunostaining for CD31 and *Rosa26*^{Ai75} Cre reporter signal in nasal mucosa of P21 control (*Bmx-Cre*^{ERT2}; *Alk1*$^{fx/+}$) and *Alk1*^{iΔAEC} mice (25μg tamoxifen on P2). Blue dashed line indicates the most dorsal crease of the nasal cavity. Caudal (C), rostral (R), dorsal (D), and ventral (V) directions are indicated.

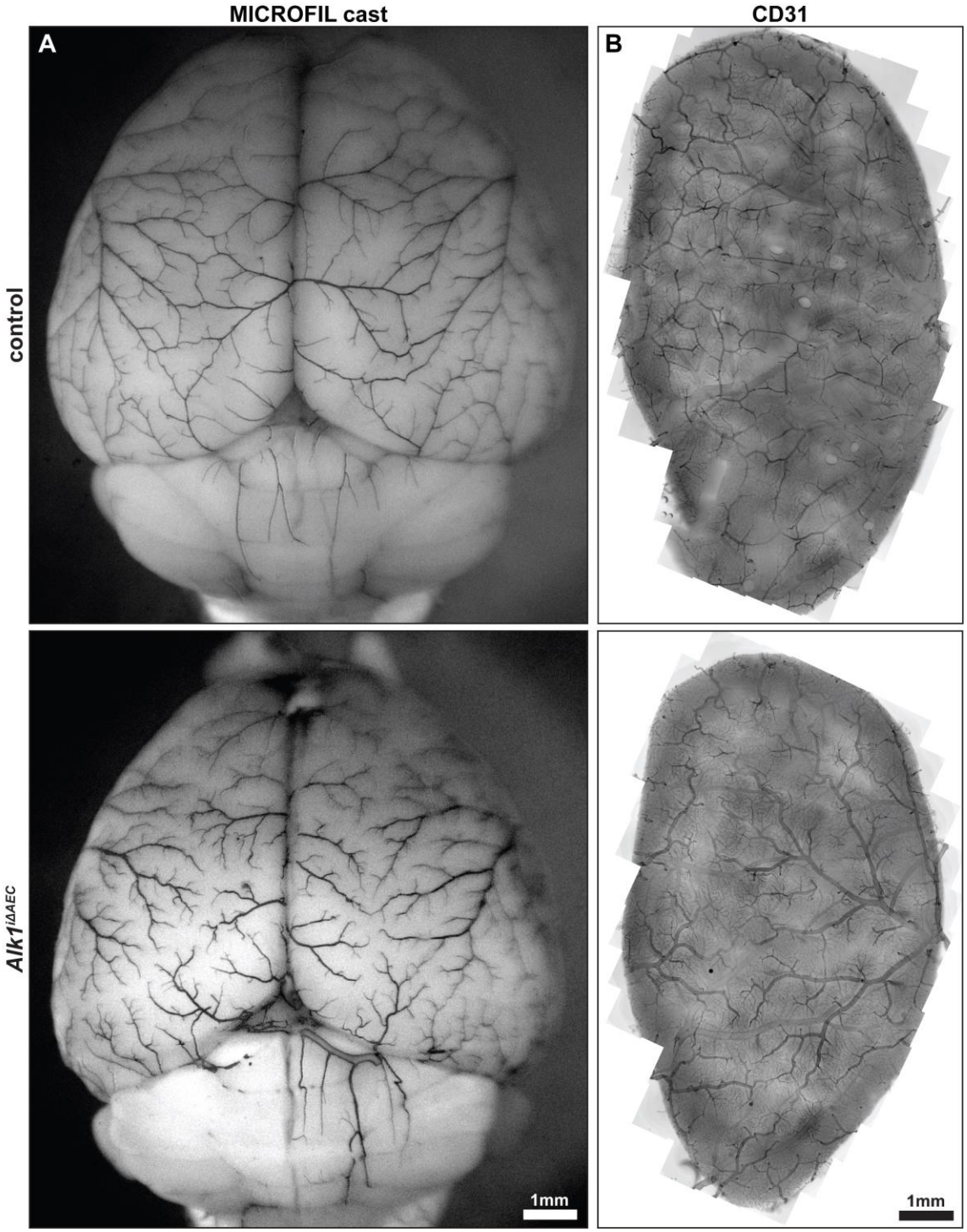

Fig. 5 | *Alk1*$^{i\Delta AEC}$ mice exhibited tortuous cerebral vasculature. (A) MICROFIL casting of the brain demonstrating tortuous vessels in control and *Alk1*$^{i\Delta AEC}$ mice at P24 (100µg tamoxifen on P2 & P3). **(B)** Wholemount immunostaining for CD31 in cerebral cortex slices of P31 control and *Alk1*$^{i\Delta AEC}$ mice (75µg tamoxifen on P2).

similar smooth muscle defect with gaps in coverage and disruption of the stereotyped circumferential vSMC alignment (**Fig. 6B**). In summary, these data reveal a novel connection between arterial endothelial expression of ALK1 and the proper ensheathing and function of vascular smooth muscle in the nose and brain.

Alk1$^{i\Delta AEC}$ mouse vasculature exhibited decreased expression of arterial marker *Efnb2*.

Disruption of vascular smooth muscle coverage on arteries is often associated with the loss of endothelial arterial identity (reviewed in [39]). To investigate whether *Alk1*$^{i\Delta AEC}$ mice exhibit loss of arterial identity in arteries in the nose and brain

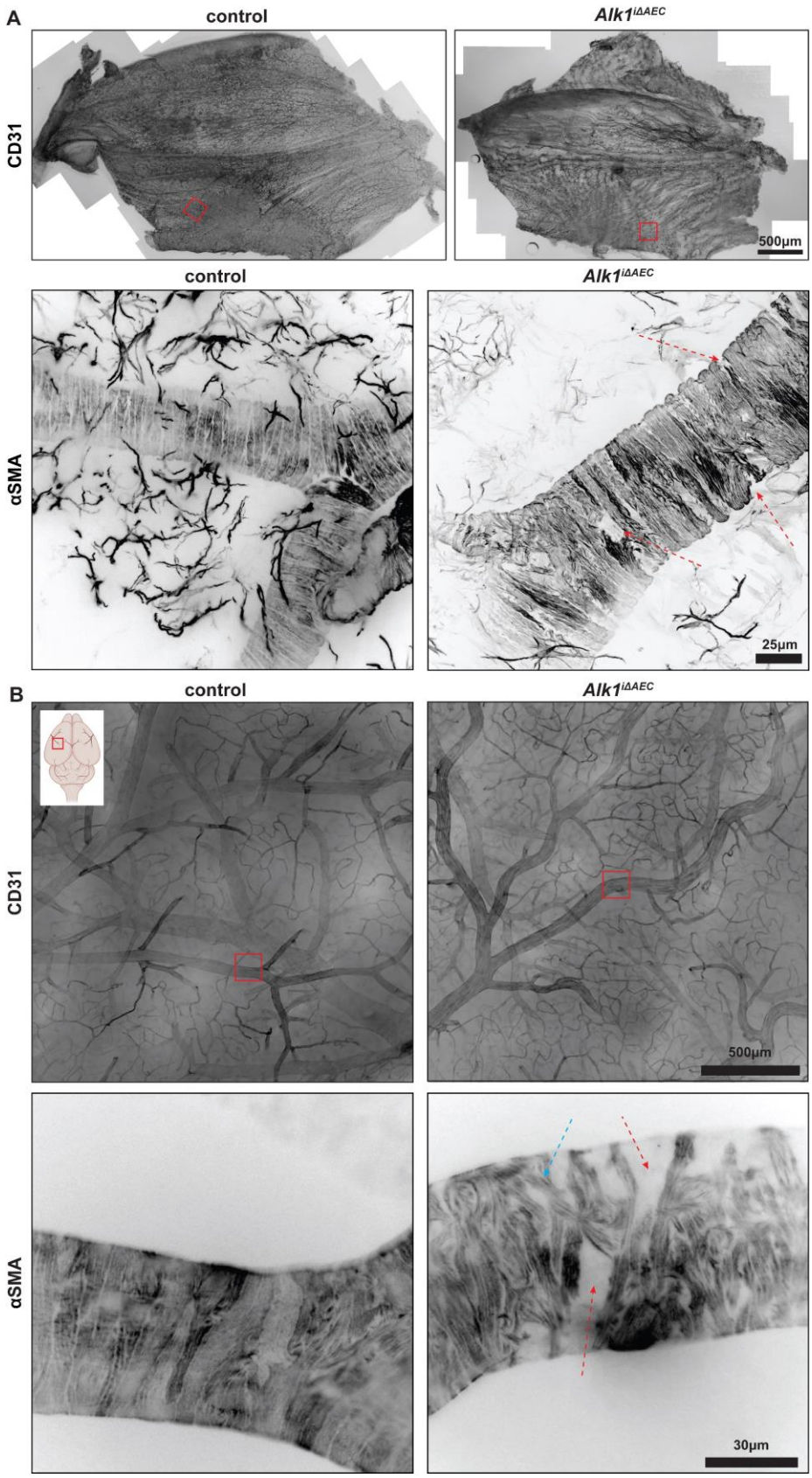

Fig. 6 | *Alk1*$^{i\Delta AEC}$ mice exhibited disorganized smooth muscle coverage of the nasal and cerebral vasculature. (A) Wholemount immunostaining for CD31 and α-smooth muscle actin (αSMA) in nasal mucosa of P103 control and *Alk1*$^{i\Delta AEC}$ mice (100μg tamoxifen per g body weight on P13 & P14). **(B)** Photomicrographs of wholemount immunostaining for CD31 and αSMA in cerebral cortex slices of P31 control and *Alk1*$^{i\Delta AEC}$ mice (75μg tamoxifen on P2). Red arrows indicate gaps in smooth muscle coverage. Blue arrow indicates regions of misaligned smooth muscle cells. Brain schematic created in BioRender.com.

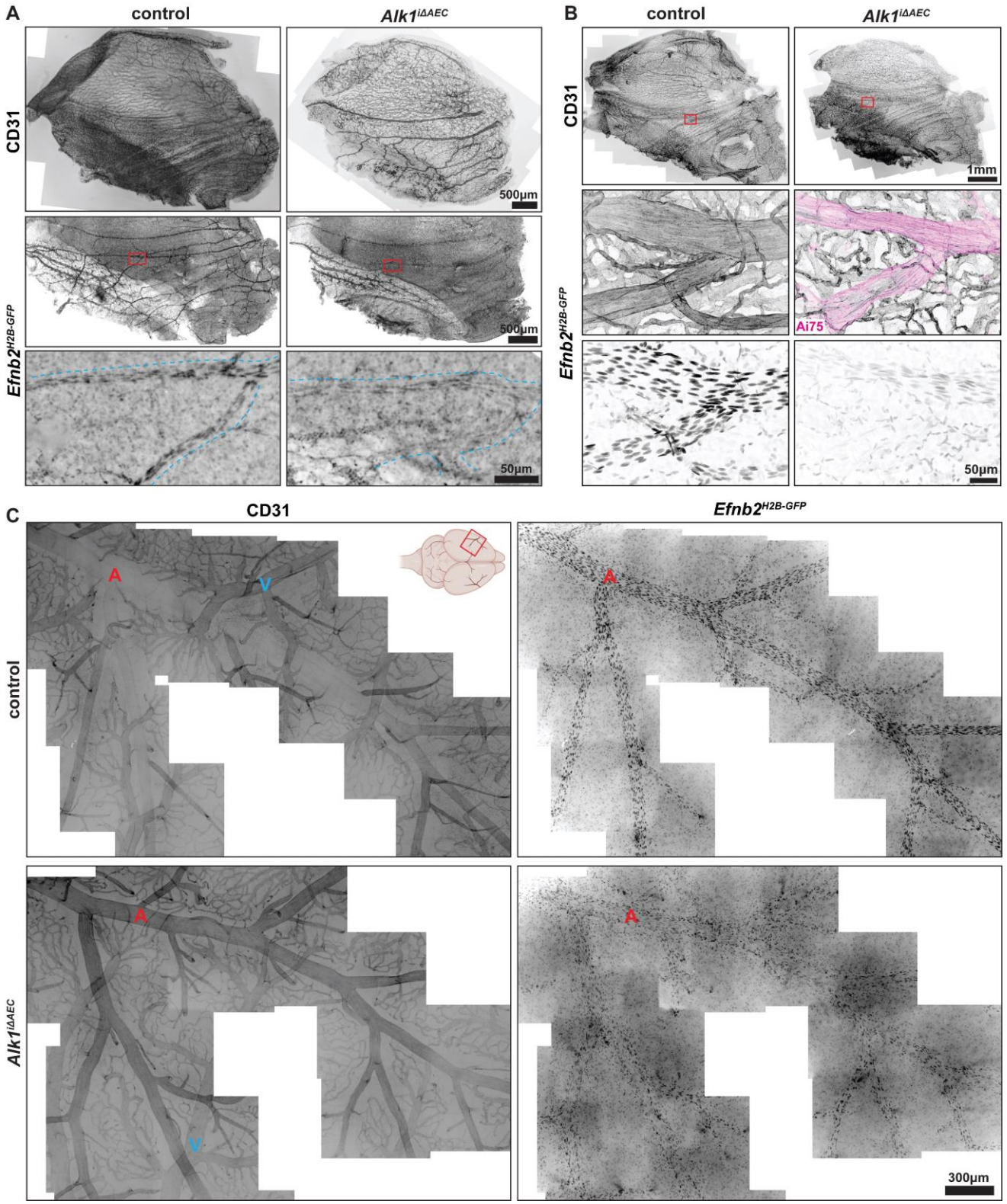

Fig. 7 | *Alk1*$^{i\Delta AEC}$ mice exhibited downregulation of arterial marker *Efnb2* expression in the nasal and cerebral arterial vasculature. (A) Wholemount immunostaining for CD31 and expression of *Efnb2*$^{H2B\text{-}GFP}$ arterial endothelial reporter in nasal mucosa of P13 control and *Alk1*$^{i\Delta AEC}$ mice (100µg tamoxifen per g body weight on P13 & P14). Red boxed indicates location of inset images. Black dashed line indicates position of artery. **(B)** Wholemount immunostaining for CD31 and expression of *Rosa26*^{Ai75} Cre recombinase reporter and *Efnb2*$^{H2B\text{-}GFP}$ arterial endothelial reporter in nasal mucosa of P13 control and *Alk1*$^{i\Delta AEC}$ mice (25µg tamoxifen on P2). Red boxed indicates location of inset images. **(C)** Wholemount immunostaining for CD31 and expression of *Efnb2*$^{H2B\text{-}GFP}$ arterial endothelial reporter in cerebral cortex slices of P13 control and *Alk1*$^{i\Delta AEC}$ mice (25µg tamoxifen on P2). Mouse schematic created in BioRender.com. A and V label arteries and veins, respectively.

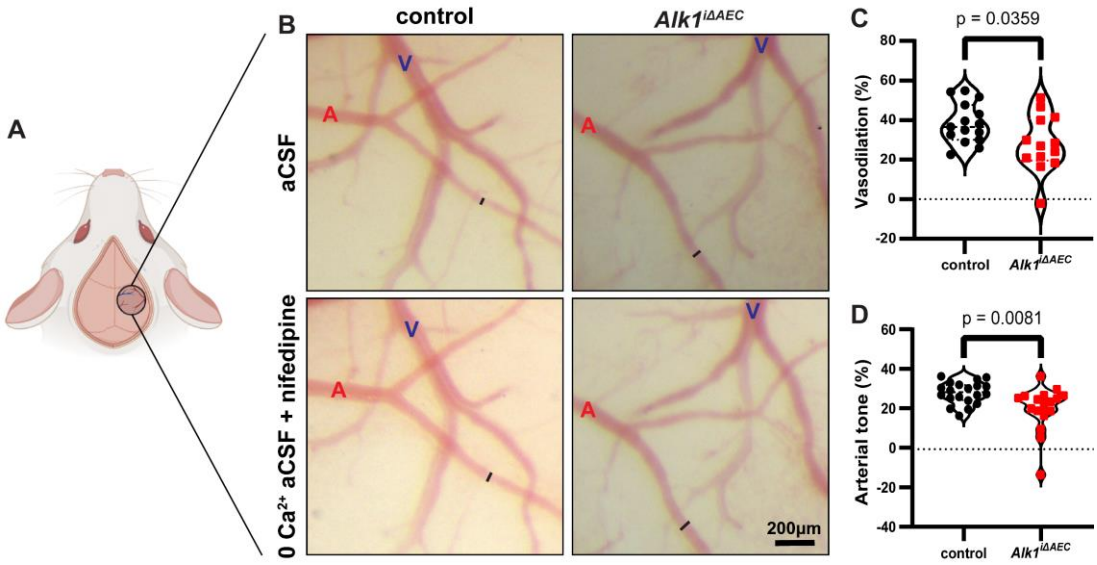

Fig. 8 | *Alk1*$^{i\Delta AEC}$ mice exhibited impaired in vivo cerebral vascular tone and significant changes in acetylcholine-induced vasodilation in arteries. **(A)** Schematic demonstrating location of pial vessel imaging during in vivo arterial tone assay. **(B)** Representative images of pial vasculature in live P13 control and *Alk1*$^{i\Delta AEC}$ mice (100μg tamoxifen on P2 & P3) visualized through an open cranial window. aCSF, artificial cerebrospinal fluid. **(C)** Quantification of changes in acetylcholine-induced vasodilation between control and *Alk1*$^{i\Delta AEC}$ mice (unpaired Student's t-test). **(D)** Quantification of changes in arterial tone between control and *Alk1*$^{i\Delta AEC}$ mice (Mann-Whitney U test).

where severe vSMC disorganization was identified, we examined the expression of the *Efnb2*$^{H2B\text{-}GFP}$ arterial endothelial reporter allele. As expected, in control mice we observed widespread expression of H2B-GFP in the arterial vessels; however, in *Alk1*$^{i\Delta AEC}$ mice we observed loss or significant reduction in expression in some arterial branches in both the nasal mucosa (**Fig. 7A, B**) and brain and (**Fig. 7C**). The vessels exhibiting changes in *Efnb2*$^{H2B\text{-}GFP}$ expression were the arteries which had undergone Cre-mediated recombination and loss of ALK1, as demonstrated by expression of the *Rosa26*^{Ai75} Cre recombinase reporter (**Fig. 7B**). Together, these data indicate that arterial endothelial loss of ALK1 results in decreased arterialization of arteries as demonstrated by expression of the arterial identity marker EphrinB2.

***Alk1*$^{i\Delta AEC}$ mice exhibited impaired cerebral vascular constriction and acetylcholine-induced vasodilation.**
Recent work from our group has identified a key role for dysregulation of arterial tone in the developmental pathophysiology of arteriovenous malformations, which are high-flow vascular anomalies that shunt blood directly from arteries to veins by displacing intervening capillaries, capable of causing both hemorrhage and ischemia[40–42]. Given the vessel enlargement and defects in vSMC organization, we hypothesized that arteries in *Alk1*$^{i\Delta AEC}$ mice exhibit defects in regulation of arterial tone, or the degree of vascular constriction and dilation.

Using an established in vivo assay for assessment of arterial tone[40,43], we measured diameters of pial arteries through an open cranial window in anesthetized *Alk1*$^{i\Delta AEC}$ and control mice. We measured vessel diameters at baseline with topical administration of artificial cerebrospinal fluid (aCSF), in a vasodilated state with aCSF containing acetylcholine, and at a maximally dilated state with aCSF devoid of Ca^{2+} and containing 1 μM of the L-type Ca^{2+} channel antagonist, nifedipine. Acetylcholine-induced vasodilation is a measure of the pial artery vasodilation in response to endothelial nitric oxide synthase (eNOS) activation, whereas nifedipine maximal dilation is a measure of the arterial dilation when L-type calcium ion channels have been inhibited and vSMCs fail to contract. We found both acetylcholine-induced vasodilation and tone of pial arteries to be reduced in the *Alk1*$^{i\Delta AEC}$ mice relative to controls with the baseline dilation being significantly greater than that of controls (**Fig. 8**). Together, these results identify a key role of arterial endothelial ALK1 in the regulation of cerebrovascular contractility and acetylcholine-induced vasodilation.

Discussion

Here, we report that somatic mutation of *Alk1/Hht2* in primarily arterial endothelial cells is sufficient for the formation of hemorrhagic vascular malformations in the nose and brain. We show that in both the nasal mucosa and brain, arterial endothelial ALK1 loss results in vessel enlargement and tortuosity. We demonstrate that this tortuosity is accompanied by disorganization of vascular smooth muscle coverage, loss of arterial identity, and defects in vasoregulation. Taken together, these data demonstrate that somatic ALK1 loss in arterial endothelial cells of mice can cause hemorrhagic vascular malformations, providing a critically needed preclinical model to study HHT-associated epistaxis, and delineating a previously unappreciated arterial contribution to HHT pathophysiology.

In our study, 47.6% of the cages containing *Alk1*$^{i\Delta AEC}$ mice showed evidence of nose bleeding, such as blood on the walls or bedding. Given the transient nature of the bleeding episodes and the propensity of mice to clean themselves quickly, our detection likely underestimates the

true frequency of nosebleeds in these animals. This model presents a significant advancement as it is, to the best of our knowledge, the first mouse model of HHT that exhibits epistaxis, one of the most clinically significant and debilitating symptoms of HHT[9].

We demonstrate by ALK1 immunostaining in the cerebral cortex that the *Bmx(PAC)-Cre*^{ERT2} exhibits activity specific to the arterial endothelium. Unfortunately, it is technically difficulty to achieve satisfactorily low noise ALK1 immunostaining in nasal mucosa. However, single-cell transcriptomic analysis of vascular heterogeneity in the mouse nasal mucosa demonstrates that *Bmx* expression in the nasal mucosa is largely specific to the arterial endothelium[44], supporting our use of *Bmx(PAC)-Cre*^{ERT2} to model arterial endothelial *Alk1* mutation in the nasal vasculature.

Notably, 72.4% of *Alk1*^{iΔAEC} mice developed multifocal microhemorrhages in the brain, though no symptoms of neurodysfunction were detected. Likewise, brain AVMs in HHT patients are smaller, multifocal, and often do not require surgical intervention due to minimal symptomatic burden[34,45]. Our finding of multifocal asymptomatic hemorrhages in *Alk1*^{iΔAEC} brains, closely mirrors human HHT manifestation.

We titrated tamoxifen dosing as an effective strategy to develop the optimal *Alk1*^{iΔAEC} mice for modeling HHT phenotypes. While mice dosed with high doses of tamoxifen exhibited premature moribundity (median 23 days), we found that *Alk1*^{iΔAEC} mice with a lower dose did not exhibit obviously abnormal behaviors besides spontaneous epistaxis. Importantly, *Alk1*^{iΔAEC} mice, like HHT patients, develop compensatory cardiomegaly likely due to a decrease in peripheral vascular resistance. The ability to model spontaneous epistaxis without premature illness makes *Alk1*^{iΔAEC} mice an ideal preclinical model for both basic discovery and therapeutic development.

MICROFIL casting revealed the enlarged tortuous nasal vessels in *Alk1*^{iΔAEC} mice. We further obtained the first immunostaining images of the nasal mucosa of mice with mutant HHT genes and uncovered enlarged and tortuous vessels in the vasculature of the *Alk1*^{iΔAEC} mucosa covering the nasal septum. We believe that this vascular bed in the mouse is analogous to Little's area in humans, where the majority of epistaxis events originate[10]. These aberrant vessels in the nasal mucosa are likely the sources of severe epistaxis in *Alk1*^{iΔAEC} mice.

MICROFIL casting and immunostaining of the cerebral cortex of *Alk1*^{iΔAEC} and control mice also revealed vessel tortuosity and other vascular defects accompanying the multifocal cerebral vascular hemorrhages. We do note, however, that the defects in vascular organization of the brain appear to be less pronounced than those of the nasal mucosa, which mirrors the fact that HHT patients develop nasal telangiectasias much more frequently than cerebrovascular AVMs[46].

Normal function of vascular smooth muscle, is critical for vessel integrity and its disruption is associated with vascular hemorrhage[47,48]. Thinning of the tunica media in nasal vasculature of people with chronic nosebleeds has been

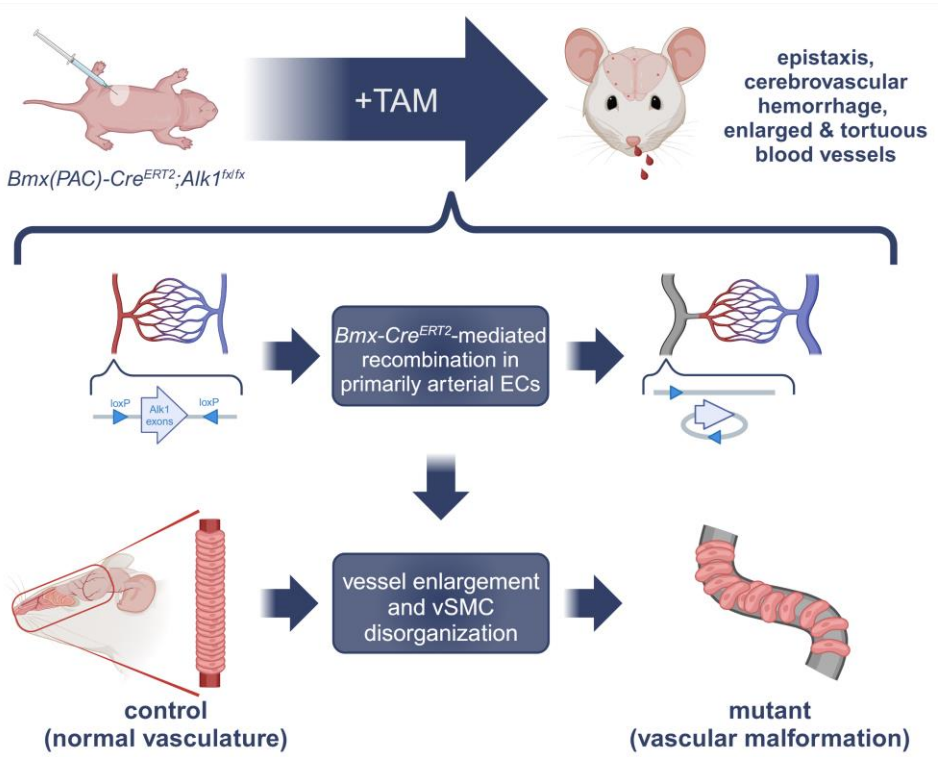

Fig. 9 | Schematic overview detailing phenotypic consequences of somatic Alk1 mutation in arterial endothelial cells. Conceptual summary of approach and phenotypes in *Alk1*^{iΔAEC} mice. Created in BioRender.com.

described comprehensively by electron and light microscopy of nasal mucosal biopsies[49], indicating that smooth muscle dysfunction may be a precursor to epistaxis. We found that the tortuous blood vessels were accompanied by defective smooth muscle coverage characterized by loss of the compact, radial alignment in *Alk1*$^{i\Delta AEC}$ mice. This abnormal ensheathing of the artery likely predisposes this site to hemorrhage. Thus, the vSMC defect in the arteries of *Alk1*$^{i\Delta AEC}$ mice likely plays a critical role in the progression of the malformation and predisposing the vessels to hemorrhage.

Endothelial *Alk1* deletion leading to smooth muscle dysreregulation is supported by endothelial *L1cre* mediated *Alk1* deletion, which results in severe enlargement of the vitelline artery/vein and medial wall thinning of the vitelline artery and embryonic lethality[19]. It is well known changes from the vascular endothelium can affect vSMC differentiation and function[50,51]. It is also well established that loss of vSMC integrity is a major risk for vessel rupture[52]. Taken together these data support that endothelial ALK1 plays a critical role regulating smooth muscle coverage, which when disrupted is a pathological mechanism for epistaxis.

How loss of arterial endothelial ALK1 compromised smooth muscle coverage remains to be elucidated. It is possible that endothelial arterial specification is integral to vSMC coverage. *Alk1*$^{i\Delta AEC}$ arteries lose arterial identity, thus develop defective vSMC coverage. Supporting this notion, we demonstrated downregulation of the arterial marker *Efnb2* in arteries of *Alk1*$^{i\Delta AEC}$ mice, accompanying dysfunctional smooth muscle coverage. Expression of *Efnb2* is a faithful marker for arterial endothelial specification[53–57]. ALK1 signaling induces expression of *Efnb2* and that loss of ALK1 is sufficient to downregulate Efnb2 expression[13,58,59]. Likewise, arterial specification markers *Id1* and *Hey1* are downregulated when HHT1 is deleted in the endothelium in mice [29]. It is likely that loss of ALK1 in the arterial endothelium of *Alk1*$^{i\Delta AEC}$ mice reduces arterial programming, leading to smooth muscle defects, which predispose vessels to hemorrhage. Together, these data support a model wherein ALK1 modulation of *Efnb2* is a potential mechanism underlying compromised arterial vSMC coverage and hemorrhages.

Consistent with vSMC dysfunction, we identified that arterial endothelial loss of ALK1 results in defective vasoregulation as demonstrated by reduced in vivo vascular tone and acetylcholine-induced vasodilation. These findings provide mechanistic insight into the cause of vessel enlargement and tortuosity, as the arterial contractility is disrupted. In addition, defective endothelial signaling may play a critical role in modulating vSMC functions, as increased reactive oxygen species generation is linked to compromised pulmonary artery vasomotor tone in *Alk1*$^{+/-}$ mice[60]. Given that loss of ALK1 reduced vascular tone in both brain and lung vasculature, it likely affects vascular tone in other tissues, including the nasal mucosa, where vascular tone measurement is not currently feasible.

We propose that defects in a feeding artery may contribute to the severe epistaxis experienced by HHT patients. This hypothesis is supported by previous work which found that there is no correlation between the size and the hemorrhage risk of a brain AVM, and that smaller AVMs with higher arterial feeding pressure are more prone to hemorrhage[61]. Our work underscore the need for clinical study of potential arterial lesions or defects in HHT-associated epistaxis and other bleeding manifestations.

In summary, this work demonstrates the first evidence that somatic ALK1 loss in AECs can cause hemorrhagic vascular malformations, delineating a previously unappreciated arterial contribution to HHT pathogenesis. We believe that that this work demonstrates a significant advancement of our understanding of the cellular events inciting HHT-associated epistaxis, provides new avenues to better understand the molecular determinants of vascular defects leading to the devastating bleeding in patients.

List of Supplementary Materials

Supplemental Figures 1-4
Movie S1
Supplemental Methods

References

1. Shovlin, C. L. *et al.* Diagnostic criteria for hereditary hemorrhagic telangiectasia (Rendu-Osler-Weber syndrome). *Am. J. Med. Genet.* **91**, 66–67 (2000).
2. Al Tabosh, T. *et al.* Hereditary hemorrhagic telangiectasia: from signaling insights to therapeutic advances. *J. Clin. Invest.* **134**, e176379 (2024).
3. Plauchu, H., De Chadarévian, J., Bideau, A. & Robert, J. Age-related clinical profile of hereditary hemorrhagic telangiectasia in an epidemiologically recruited population. *Am. J. Med. Genet.* **32**, 291–297 (1989).
4. Kasthuri, R. S. *et al.* Prevalence and predictors of anemia in hereditary hemorrhagic telangiectasia. *Am. J. Hematol.* **92**, (2017).
5. Köhler, S. *et al.* The Human Phenotype Ontology in 2021. *Nucleic Acids Res.* **49**, D1207–D1217 (2021).
6. Köhler, S. *et al.* The Human Phenotype Ontology project: linking molecular biology and disease through phenotype data. *Nucleic Acids Res.* **42**, D966-974 (2014).
7. Hetts, S. W., Shieh, J. T., Ohliger, M. A. & Conrad, M. B. Hereditary Hemorrhagic Telangiectasia: The Convergence of Genotype, Phenotype, and Imaging in Modern Diagnosis and Management of a Multisystem Disease. *Radiology* **300**, 17–30 (2021).
8. Garcia-Tsao, G. *et al.* Liver Disease in Patients with Hereditary Hemorrhagic Telangiectasia. *N. Engl. J. Med.* **343**, 931–936 (2000).
9. Chin, C. J., Rotenberg, B. W. & Witterick, I. J. Epistaxis in hereditary hemorrhagic telangiectasia: An evidence based review of surgical management. *J. Otolaryngol. - Head Neck Surg.* **45**, 3 (2016).
10. Little, James L. A hitherto undescribed lesion as a cause of epistaxis, with four cases. *Hosp. Gaz.* **v. 6**, 5–6 (1879).

11. Matti, E. *et al.* Nasal Endoscopy in the Clinical Diagnosis of Hereditary Hemorrhagic Telangiectasia. *J. Pediatr.* **238**, 74-79.e2 (2021).
12. Johnson, D. W. *et al.* Mutations in the activin receptor–like kinase 1 gene in hereditary haemorrhagic telangiectasia type 2. *Nat. Genet.* **13**, 189–195 (1996).
13. Urness, L. D., Sorensen, L. K. & Li, D. Y. Arteriovenous malformations in mice lacking activin receptor-like kinase-1. *Nat. Genet.* **26**, 328–331 (2000).
14. Seki, T., Yun, J. & Oh, S. P. Arterial Endothelium-Specific Activin Receptor-Like Kinase 1 Expression Suggests Its Role in Arterialization and Vascular Remodeling. *Circ. Res.* **93**, 682–689 (2003).
15. Oh, S. P. *et al.* Activin receptor-like kinase 1 modulates transforming growth factor-β1 signaling in the regulation of angiogenesis. *Proc. Natl. Acad. Sci.* **97**, 2626–2631 (2000).
16. Nielsen, C. M., Huang, L., Murphy, P. A., Lawton, M. T. & Wang, R. A. Mouse Models of Cerebral Arteriovenous Malformation. *Stroke* **47**, 293–300 (2016).
17. Arthur, H. M. & Roman, B. L. An update on preclinical models of hereditary haemorrhagic telangiectasia: Insights into disease mechanisms. *Front. Med.* **9**, 973964 (2022).
18. Srinivasan, S. *et al.* A mouse model for hereditary hemorrhagic telangiectasia (HHT) type 2. *Hum. Mol. Genet.* **12**, 473–482 (2003).
19. Park, S. O. *et al.* ALK5- and TGFBR2-independent role of ALK1 in the pathogenesis of hereditary hemorrhagic telangiectasia type 2. *Blood* **111**, 633–642 (2008).
20. Park, S. O. *et al.* Real-time imaging of de novo arteriovenous malformation in a mouse model of hereditary hemorrhagic telangiectasia. *J. Clin. Invest.* **119**, 3487–3496 (2009).
21. Baeyens, N. *et al.* Defective fluid shear stress mechanotransduction mediates hereditary hemorrhagic telangiectasia. *J. Cell Biol.* **214**, 807–816 (2016).
22. Tual-Chalot, S. *et al.* Endothelial Depletion of Acvrl1 in Mice Leads to Arteriovenous Malformations Associated with Reduced Endoglin Expression. *PLoS ONE* **9**, e98646 (2014).
23. Queisser, A., Seront, E., Boon, L. M. & Vikkula, M. Genetic Basis and Therapies for Vascular Anomalies. *Circ. Res.* **129**, 155–173 (2021).
24. Knudson, A. G. Mutation and Cancer: Statistical Study of Retinoblastoma. *Proc. Natl. Acad. Sci.* **68**, 820–823 (1971).
25. Snellings, D. A. *et al.* Somatic Mutations in Vascular Malformations of Hereditary Hemorrhagic Telangiectasia Result in Bi-allelic Loss of ENG or ACVRL1. *Am. J. Hum. Genet.* **105**, 894–906 (2019).
26. DeBose-Scarlett, E. *et al.* Somatic mutations in arteriovenous malformations in hereditary hemorrhagic telangiectasia support a bi-allelic two-hit mutation mechanism of pathogenesis. *Am. J. Hum. Genet.* **111**, 2283–2298 (2024).
27. Park, H. *et al.* Defective Flow-Migration Coupling Causes Arteriovenous Malformations in Hereditary Hemorrhagic Telangiectasia. *Circulation* **144**, 805–822 (2021).
28. Singh, E., Redgrave, R. E., Phillips, H. M. & Arthur, H. M. Arterial endoglin does not protect against arteriovenous malformations. *Angiogenesis* **23**, 559–566 (2020).
29. Jin, Y. *et al.* Endoglin prevents vascular malformation by regulating flow-induced cell migration and specification through VEGFR2 signalling. *Nat. Cell Biol.* **19**, 639–652 (2017).
30. Rochon, E. R., Menon, P. G. & Roman, B. L. Alk1 controls arterial endothelial cell migration in lumenized vessels. *Dev. Camb. Engl.* **143**, 2593–2602 (2016).
31. Lee, H.-W. *et al.* Role of Venous Endothelial Cells in Developmental and Pathologic Angiogenesis. *Circulation* **144**, 1308–1322 (2021).
32. Ekman, N. *et al.* Bmx Tyrosine Kinase Is Specifically Expressed in the Endocardium and the Endothelium of Large Arteries. *Circulation* **96**, 1729–1732 (1997).
33. Davy, A., Bush, J. O. & Soriano, P. Inhibition of gap junction communication at ectopic Eph/ephrin boundaries underlies craniofrontonasal syndrome. *PLoS Biol.* **4**, e315 (2006).
34. Maher, C. O., Piepgras, D. G., Brown, R. D., Friedman, J. A. & Pollock, B. E. Cerebrovascular Manifestations in 321 Cases of Hereditary Hemorrhagic Telangiectasia. *Stroke* **32**, 877–882 (2001).
35. Bourgeois, N. *et al.* Osler-Weber-Rendu disease associated with hepatic involvement and high output heart failure. *J. Clin. Gastroenterol.* **12**, 236–238 (1990).
36. Hyldahl, S. J., El-Jaji, M. Q., Schuster, A. & Kjeldsen, A. D. Skin and mucosal telangiectatic lesions in hereditary hemorrhagic telangiectasia patients. *Int. J. Dermatol.* **61**, 1497–1505 (2022).
37. Callewaert, B., De Paepe, A. & Coucke, P. Arterial Tortuosity Syndrome. in *GeneReviews®* (eds. Adam, M. P. et al.) (University of Washington, Seattle, Seattle (WA), 1993).
38. Morris, S. A. *et al.* Increased Vertebral Artery Tortuosity Index Is Associated With Adverse Outcomes in Children and Young Adults With Connective Tissue Disorders. *Circulation* **124**, 388–396 (2011).
39. Jaminon, A., Reesink, K., Kroon, A. & Schurgers, L. The Role of Vascular Smooth Muscle Cells in Arterial Remodeling: Focus on Calcification-Related Processes. *Int. J. Mol. Sci.* **20**, 5694 (2019).
40. Huang, L. *et al.* Nitric oxide synthase and reduced arterial tone contribute to arteriovenous malformation. *Sci. Adv.* **9**, eade7280 (2023).
41. Lawton, M. T. *et al.* Brain arteriovenous malformations. *Nat. Rev. Dis. Primer* **1**, 15008 (2015).
42. Friedlander, R. M. Clinical practice. Arteriovenous malformations of the brain. *N. Engl. J. Med.* **356**, 2704–2712 (2007).
43. Syed, A. U. *et al.* Adenylyl cyclase 5-generated cAMP controls cerebral vascular reactivity during diabetic hyperglycemia. *J. Clin. Invest.* **129**, 3140–3152 (2019).
44. Hong, S. P. *et al.* Three-dimensional morphologic and molecular atlases of nasal vasculature. *Nat. Cardiovasc. Res.* **2**, 449–466 (2023).
45. Yang, W. *et al.* Lower Risk of Intracranial Arteriovenous Malformation Hemorrhage in Patients With Hereditary Hemorrhagic Telangiectasia. *Neurosurgery* **78**, 684–693 (2016).
46. Sautter, N. B. & Smith, T. L. Hereditary hemorrhagic telangiectasia–related epistaxis: innovations in understanding and management. *Int. Forum Allergy Rhinol.* **2**, 422–431 (2012).
47. Takebayashi, S. & Kaneko, M. Electron microscopic studies of ruptured arteries in hypertensive intracerebral hemorrhage. *Stroke* **14**, 28–36 (1983).
48. Van Den Akker, N. M. S. *et al.* PDGF-B signaling is important for murine cardiac development: Its role in developing atrioventricular valves, coronaries, and cardiac innervation. *Dev. Dyn.* **237**, 494–503 (2008).
49. Johansson, B. R., Beran, M. & Petrusson, B. Light and Electron Microscopy of Varicose Vessels and Telangiomas in the Nasal Mucosa of Habitual Nosebleeders. *Acta Otolaryngol. (Stockh.)* **99**, 620–629 (1985).
50. Owens, G. K., Kumar, M. S. & Wamhoff, B. R. Molecular regulation of vascular smooth muscle cell differentiation in development and disease. *Physiol. Rev.* **84**, 767–801 (2004).
51. Majesky, M. W. Vascular Smooth Muscle Cells. *Arterioscler. Thromb. Vasc. Biol.* **36**, (2016).

52. Gerosa, C. *et al.* The human carotid atherosclerotic plaque: an observational review of histological scoring systems. *Eur. Rev. Med. Pharmacol. Sci.* **27**, 3784–3792 (2023).
53. Stewen, J. *et al.* Eph-ephrin signaling couples endothelial cell sorting and arterial specification. *Nat. Commun.* **15**, 2539 (2024).
54. Wang, H. U., Chen, Z.-F. & Anderson, D. J. Molecular Distinction and Angiogenic Interaction between Embryonic Arteries and Veins Revealed by ephrin-B2 and Its Receptor Eph-B4. *Cell* **93**, 741–753 (1998).
55. Murphy, P. A. *et al.* Constitutively active Notch4 receptor elicits brain arteriovenous malformations through enlargement of capillary-like vessels. *Proc. Natl. Acad. Sci.* **111**, 18007–18012 (2014).
56. Murphy, P. A. *et al.* Endothelial Notch4 signaling induces hallmarks of brain arteriovenous malformations in mice. *Proc. Natl. Acad. Sci. U. S. A.* **105**, 10901–10906 (2008).
57. Nielsen, C. M. *et al.* Deletion of Rbpj from postnatal endothelium leads to abnormal arteriovenous shunting in mice. *Development* **141**, 3782–3792 (2014).
58. Sorensen, L. K., Brooke, B. S., Li, D. Y. & Urness, L. D. Loss of distinct arterial and venous boundaries in mice lacking endoglin, a vascular-specific TGFbeta coreceptor. *Dev. Biol.* **261**, 235–250 (2003).
59. Kim, J.-H., Peacock, M. R., George, S. C. & Hughes, C. C. W. BMP9 induces EphrinB2 expression in endothelial cells through an Alk1-BMPRII/ActRII-ID1/ID3-dependent pathway: implications for hereditary hemorrhagic telangiectasia type II. *Angiogenesis* **15**, 497–509 (2012).
60. Jerkic, M. *et al.* Pulmonary hypertension in adult Alk1 heterozygous mice due to oxidative stress. *Cardiovasc. Res.* **92**, 375–384 (2011).
61. Spetzler, R. F. *et al.* Relationship of perfusion pressure and size to risk of hemorrhage from arteriovenous malformations. *J. Neurosurg.* **76**, 918–923 (1992).

Materials and methods

Mice

Animals were maintained and treated in accordance with guidelines of the University of California San Francisco Institutional Animal Care and Use Committee with approved protocol AN183040. *Bmx-Cre*^{ERT2} (MGI: 5513853), *ROSA26*^{Ai75} (MGI: 5603432), *Alk1*^{fx} (MGI: 4398904), and *Efnb2*$^{H2B\text{-}GFP}$ (MGI: 3526818) alleles have been published[19,33,62,63]. The genetic background of the mice used in this study was mixed C57BL6/J and FVB/N. Both male and female mice were used for experiments.

Tamoxifen (25, 50, 75, or 100µg; Sigma, T5648) diluted in peanut oil (Fisher Scientific, S25760) was injected intragastrically into the P2 mice unless otherwise noted. Mice injected at P13 and P14 were injected intraperitoneally with 100 µg tamoxifen per g body weight. Moribundity was determined by trained veterinary nurses in accordance with the NIH Office of Animal Care and Use guidelines. Veterinary nurses were blind to any experimental information.

Gross pathology

Mice were anesthetized using isofluorane were exsanguinated by transcardial perfusion of PBS followed by 1% PFA. Organs, including the brain and heart, were dissected and fixed in 10% normal buffered formalin overnight at 4°C. To examine skin, fur was removed using hair removal cream according to manufacturer protocol.

Vascular casting

Mice were anesthetized using isofluorane and were exsanguinated by transcardial perfusion of PBS followed by 1% PFA. MICROFIL:diluent:curing agent (5:4:1) was cast through the aorta. MICROFIL cast was allowed to cure at room temperature for 45 minutes and tissue was harvested, and fixed in 10% neutral buffered formalin overnight at 4°C. After serial dehydration in 25, 50, 75, and 100% ethanol at room temperature at one day intervals, tissue was then cleared in methylsalicylate before imaging. Images were captured using dissection scope and Leica LAS software.

Fluorescent probes and immunostaining

Brains[40] were dissected and whole-mount stained according to published protocols. Dissection and preparation of nasal mucosa is described in the Supplemental Methods. Samples were incubated in primary antibody overnight 4°C, washed three times with PBST (PBS with 0.1% Triton X-100), incubated with secondary antibody for 1hr at room temperature, again washed three times with PBST, and then mounted for imaging.

Antibodies and fluorescent probes used in this study include: (1) rat anti-CD31 (BD Pharmingen 555370; 1:500 dilution), (2) mouse anti-α-smooth muscle actin-Cy3-conjugated antibody (Sigma, C6198/F3777; 1:2000 dilution), (3) mouse anti-α-smooth muscle actin-Alexa Fluor 488-conjugated antibody (eBioscience,53-9760-82; 1:2000 dilution), (4) rat anti-VE-cadherin (BD Pharmingen, 555289, 1:200 dilution), (5) goat anti-ALK1 (R&D Systems, 1:200 dilution), (6) donkey anti-rat Alexa Fluor 488 (Invitrogen, A-11006, 1:1000 dilution), (7) donkey anti-rat Alexa Fluor 555 (Invitrogen, A21434, 1:1000 dilution), and (8) donkey anti-rat Alexa Fluor 647 (Jackson Immunoresearch Labs, 712-605-150, 1:500 dilution). For lectin perfusion, fluorescence-conjugated Lycopersicon esculentum lectin (Vector Laboratories) was injected into the inferior vena cava as previously described[56,64].

Microscopy and imaging

Images of casted tissue and gross morphology were collected using a dissection microscope and Leica LAS software. Images of immunostained tissues were captured using either an Axioskop 2 Plus microscope (Zeiss) and Slidebook software (Intelligent Imaging Innovations) or a Yokogawa CSU-W1/SoRa spinning disk confocal on a Ti2 inverted microscope stand (Nikon) using NIS Elements software (Nikon). Multiple images of each sample were stitched together using PTGui Pro (New House Internet Services BV). Fluorescence images were adjusted for brightness and contrast using ImageJ (National Institutes of Health, USA).

In vivo arterial tone and acetylcholine-induced vasodilation assay

Mice were injected with 100µg tamoxifen on P2 and P3. Arterial tone was assessed at P13 as described in Supplemental Materials and in previous work[40].

Statistics

Distributions were tested for normality using the Anderson-Darling test. Gaussian data was tested for statistical differences using a two-tailed unpaired Student's t-test. Non-Gaussian data was tested for differences using the Mann-Whitney U-test.

References

62. Ehling, M., Adams, S., Benedito, R. & Adams, R. H. Notch controls retinal blood vessel maturation and quiescence. *Development* **140**, 3051–3061 (2013).
63. Daigle, T. L. *et al.* A Suite of Transgenic Driver and Reporter Mouse Lines with Enhanced Brain-Cell-Type Targeting and Functionality. *Cell* **174**, 465-480.e22 (2018).

64. Carlson, T. R. *et al.* Endothelial expression of constitutively active Notch4 elicits reversible arteriovenous malformations in adult mice. *Proc. Natl. Acad. Sci. U. S. A.* **102**, 9884–9889 (2005).
65. Dunston, D., Ashby, S., Krosnowski, K., Ogura, T. & Lin, W. An Effective Manual Deboning Method To Prepare Intact Mouse Nasal Tissue With Preserved Anatomical Organization. *J. Vis. Exp.* 50538 (2013) doi:10.3791/50538.

Data and materials availability

All data needed to evaluate conclusions in the paper are present in the paper and/or the Supplementary Materials. Materials may be made available by corresponding author upon reasonable request.

Acknowledgements

We thank Dr. S. Paul Oh for providing the *Alk1*$^{fx/+}$ mouse strain and Dr. Ralf Adams for providing the *Bmx(PAC)-Cre*^{ERT2} mouse strain. We thank Dr. Jennifer Hwa for initiating the cross; Joseph Maurice and Brian Jaewoo Ko for assistance with capturing brain images; Seongju Kang for arterial diameter measurements in vascular tone assay; HyoJung Heo and Cherilyn Yu for sharing breeders; and Dr. Curtis Woodford for assistance with microscopy.

Funding

This work was supported by National Institutes of Health (NIH) NS113429 and NS067420, the Frank A. Campini Foundation, the Mildred V Strouss Trust, American Heart Association (AHA) GRNT 16850032, The Tobacco-Related Disease Research Program (TRDRP) funds 28IR-0067, and the Department of Defense Congressionally Directed Medical Research Programs W81XWH-16-1-0665 (to RAW); and NIH 5R25NS070680-13 (through UCSF to KPR). KAJ is supported by Tobacco Related Disease Research Program Predoctoral Fellowship T33DT6442 and the National Science Foundation Graduate Research Fellowship Program under Grant No. 2038436. The Nikon CSU-W1 SoRa microscope was obtained through NIH shared equipment grant S10OD028611-01.The contents are solely the responsibility of the authors and do not necessarily represent the views of the NIH. Any opinions, findings, and conclusions or recommendations expressed in this material are those of the author(s) and do not necessarily reflect the views of the National Science Foundation.

Competing interests

Authors declare that they have no competing interests.

Supplemental Materials

Supplemental Figures

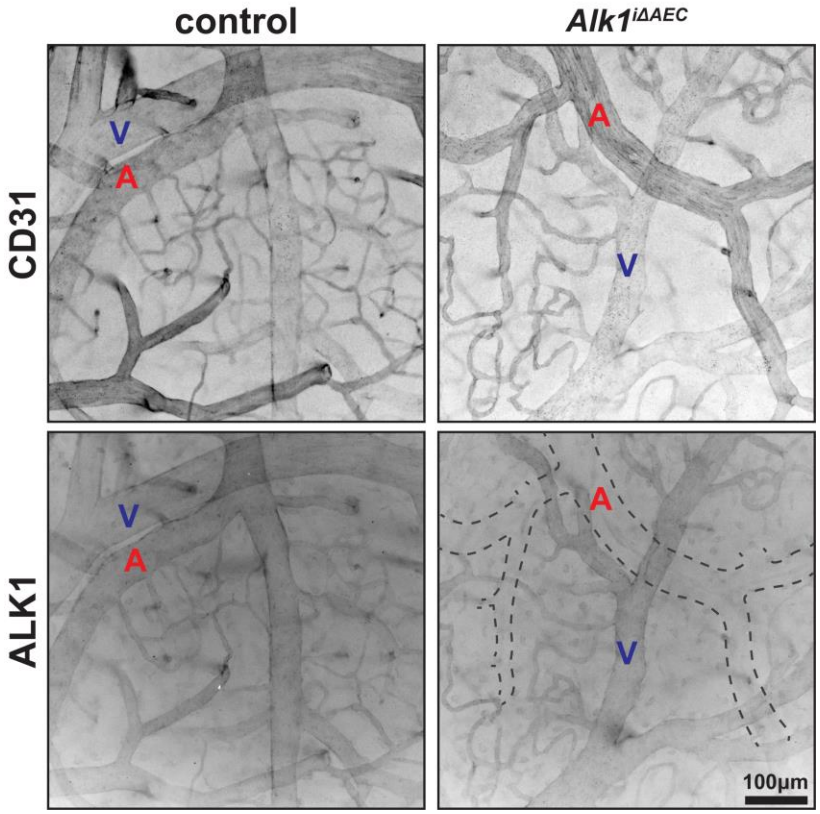

Supplemental Fig. 1 | *Bmx(PAC)-Cre^{ERT2}* mediated loss of ALK1 was restricted to arterial endothelium in *Alk1$^{i\Delta AEC}$* mice induced with high tamoxifen dose. Wholemount immunostaining for CD31 and ALK1 in cerebral cortex slices of P21 control and *Alk1$^{i\Delta AEC}$* mice (100µg tamoxifen on P2 & P3). V and A label veins and arteries, respectively.

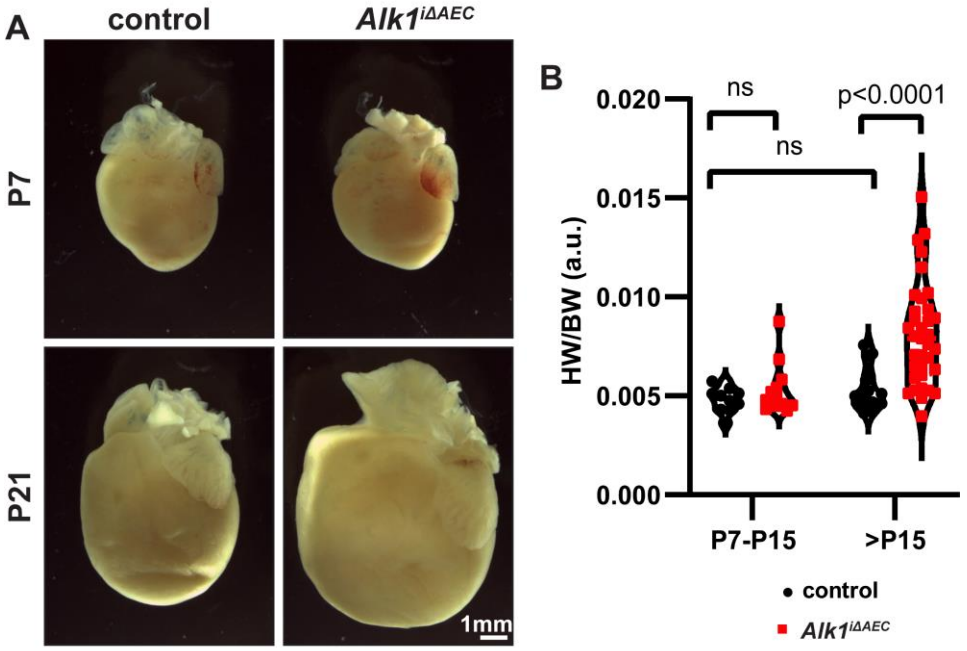

Supplemental Fig. 2 | *Alk1$^{i\Delta AEC}$* mice developed compensatory cardiomegaly. (A) Photographs of *Alk1$^{i\Delta AEC}$* and control (25µg tamoxifen on P2) hearts on P7 and P21. **(B)** Quantification of heart weight/ to body weight ratio (HW/BW) demonstrates a significant difference between control and *Alk1$^{i\Delta AEC}$* euthanized after P15, but not for mice before P15 (Mann-Whitney U test).

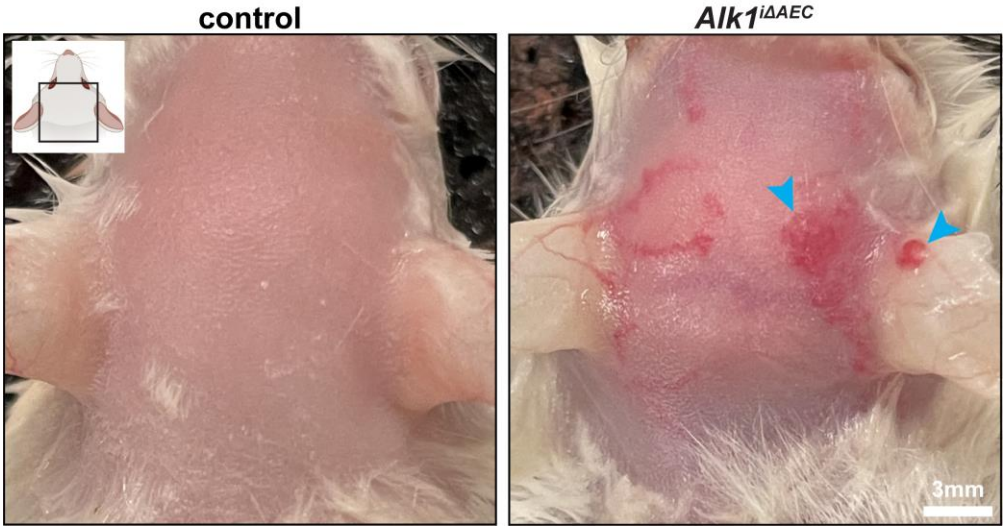

Supplemental Fig. 3 | *Alk1*$^{i\Delta AEC}$ mice developed telangiectasia-like dermal vascular malformations.
Photographs of telangiectasia-like vascular malformations (arrowheads) present in the skin of P30 *Alk1*$^{i\Delta AEC}$ (75µg tamoxifen on P2), but not control, mice. Mouse schematic created in BioRender.com.

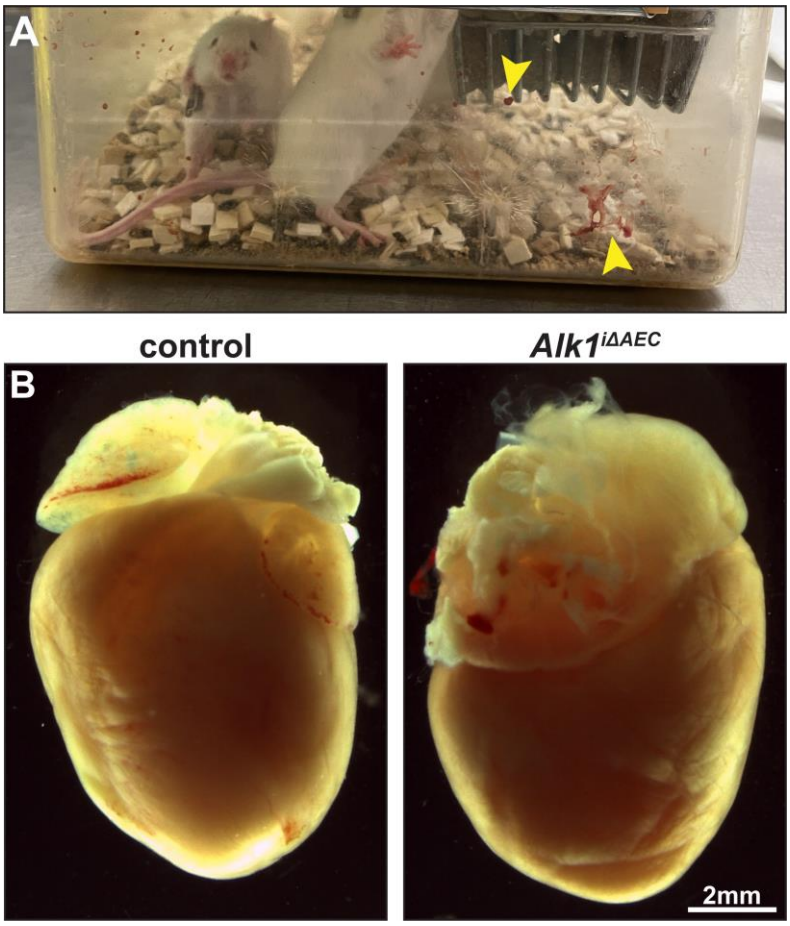

Supplemental Fig. 4 | Induction of *Bmx(PAC)-Cre^{ERT2}* at P13 and P14 induced epistaxis and cardiomegaly.
(A) Photograph of blood present (arrowheads) in cage housing *Alk1$^{i\Delta AEC}$* mice. **(B)** Photographs of *Alk1$^{i\Delta AEC}$* and control hearts on P103. All mice treated with 100µg tamoxifen per g body weight on P13 & P14.

Supplemental Movies

Supplemental Movie 1 | Epistaxis event in *Alk1*$^{i\Delta AEC}$ mouse. Video of P33 *Alk1*$^{i\Delta AEC}$ mouse (25µg tamoxifen on P2) exhibiting transient epistaxis event during handling.

Supplemental Methods

In vivo arterial tone and acetylcholine induced vasodilation assessment

A surgical anesthetic plane was achieved by intraperitoneal injection (5 µl/g mouse weight) of combined 17.5% ketamine (100 mg/ml; Dechra) and 2.5% xylazine (100 mg/ml; Bimeda) diluted in physiological saline (Hospira). Surgery was conducted as described previously[43]. Briefly, a ~2mm diameter steel plate was attached to the parietal skull using a 1:1 ratio of dental cement and cyanoacrylate glue. The head plate was secured to the holding plate, and a circular craniectomy was performed. After dura opening, first artificial cerebrospinal fluid (aCSF) and then aCSF lacking calcium but containing 1 µM L-type Ca^{2+} channel inhibitor nifedipine (called "Ca^{2+}-free aCSF + nifedipine" thereafter) were pipetted onto the exposed surface of the brain for three minutes. In some mice acetylcholine vasodilation was assessed by application of aCSF containing 10 µM acetylcholine for three minutes after the initial aCSF wash. An image was acquired and the acetylcholine was then washed out with fresh aCSF for 3 minutes. After washing, nifedipine tone was assessed described above. Images were acquired using a stereo microscope (Leica MZ12.5) with an attached camera (Zeiss AxioCam ICc5). Pial arteries were identified and analyzed using ImageJ [National Institutes of Health (NIH)]. Two locations in the arteries were analyzed per mouse. The diameters of arteries in each mouse were quantified, and results for the vascular tone and acetylcholine vasodilation in each mouse were averaged for comparison. Arterial tone was expressed as a decrease in diameter relative to the diameter obtained when incubated in Ca^{2+}-free aCSF + nifedipine (1 µM): [$(D2 - D1)/D2 \times 100\%$, where $D2$ = diameter in Ca^{2+}-free aCSF + nifedipine and $D1$ = diameter in aCSF]. Acetylcholine-induced vasodilation was expressed as the percentage change in diameter before and after ACh treatment: [$(D2 - D1)/D1 \times 100\%$, where $D2$ is diameter after ACh treatment and $D1$ is diameter before ACh treatment].

Preparation of nasal mucosa for immunostaining

Method was modified from published approaches[44,65]. For whole-mount preparation of the nasal mucosa, the associated skin and muscles were first stripped from the face. The skull, brain, and mandible were removed, and a blade was used to loosen the medial suture between the right and left nasal bones. Both sides of the nasal bones were gently moved and cut off at the rostral end from the underlying tissue. The anterior maxilla and frontal bone were dissected out with scissors, and the nasal mucosa along with the septum were lifted from the zygomatic bone using forceps. After removing the surrounding bones, the septum was gently gripped and removed from the nasal mucosa with fine forceps. The nasal mucosa was then fixed with 2% PFA for 2 hours at 4°C and permeabilized and blocked with blocking buffer containing 5% donkey serum in 1% Triton-X 100 in PBS overnight at 4°C. After completing immunostaining, the left and right nasal cavities were separated by cutting down the midline and then turbinate and septum mucosa were flattened and mounted for imaging.

References

65. Dunston, D., Ashby, S., Krosnowski, K., Ogura, T. & Lin, W. An Effective Manual Deboning Method To Prepare Intact Mouse Nasal Tissue With Preserved Anatomical Organization. *J. Vis. Exp.* 50538 (2013) doi:10.3791/50538.